Research Article Vol. 35, No. 1 / January 2018 / Journal of the Optical Society of America B 95

Journal of the Optical Society of America B

OPTICAL PHYSICS

Tunable Raman gain in mid-IR waveguides

A. D. Sánchez,[1,3,*] S. M. Hernandez,[1] J. Bonetti,[1,3] P. I. Fierens,[2,3] and D. F. Grosz[1,3]

[1]Grupo de Comunicaciones Ópticas, Instituto Balseiro, Bariloche, Río Negro 8400, Argentina
[2]Grupo de Optoelectrónica, Instituto Tecnológico de Buenos Aires, CABA 1106, Buenos Aires, Argentina
[3]Consejo Nacional de Investigaciones Científicas y Técnicas (CONICET), Buenos Aires, Argentina
*Corresponding author: alfredo.sanchez@ib.edu.ar

Received 5 September 2017; revised 10 November 2017; accepted 16 November 2017; posted 16 November 2017 (Doc. ID 305979); published 12 December 2017

By means of theoretical analysis and numerical simulations, we show a tunable Raman gain which may find applications in a variety of fields, ranging from mid-IR fiber Raman lasers and supercontinuum generation to ultra-wideband slow-light Raman-based devices. In particular, by analyzing the interplay among Raman gain, dispersion, and self-steeping (SE) in a full model of modulation instability (MI) in waveguides, we show that there exists a range of pump powers where the gain spectrum is not only dominated by the Raman contribution, but also, most strikingly, it can be fine-tuned at will. We present analytical and numerical results, in excellent agreement, confirming this observation.

OCIS codes: (190.5650) Raman effect; (190.0190) Nonlinear optics.

https://doi.org/10.1364/JOSAB.35.000095

1. INTRODUCTION

The phenomenon of modulation instability (MI) has been known and thoroughly studied for many years in numerous areas of science. In the realm of optical fibers MI plays a fundamental role, as it is intimately connected to the appearance of optical solitons and the phase-matching of four-wave mixing processes in the anomalous dispersion region [1–4]. Modulation instability also is at the heart of the occurrence of efficient parametric optical processes, which are relied upon to achieve bright and coherent light in various spectral ranges. In recent years, nonlinear phenomena such as supercontinuum generation [5,6] and rogue waves [7–12] have rekindled the interest in MI in optical fibers.

Full and tractable scalar models of MI in waveguides, see, e.g., [13,14] and references therein, can be used to analyze the complex interplay between high-order dispersion, Raman scattering, and self-steepening. In particular, Shukla and Rasmussen [15] revealed a pump power level that maximizes the MI gain, and De Angelis *et al.* [16] further revealed a power cutoff, enabled by self-steepening, above which the MI gain vanishes, leaving behind only the Raman contribution.

In this paper, we explore the region close to this MI cutoff power, at first seeking to characterize the Raman response of the transmitting waveguide. A direct measure of this response can be performed by injecting a CW pump together alongside wideband low-amplitude noise, a real-case scenario, as it accounts for the finite signal-to-noise ratio of the pump laser. In a similar vein, Raman gain in optical fibers has been measured by fitting theoretical predictions to the spectrum of backscattered amplified spontaneous emission (ASE) [17]. Intuitively, one would expect the noise spectral density to follow the Raman gain provided by the medium (as long as the pump is weakly depleted). We show that this is indeed the case in the normal dispersion region. However, in the anomalous dispersion region an unexpected behavior emerges. Beyond the MI cutoff power, where the medium response is dominated by the Raman contribution, a tunable gain is observed. Moreover, the central frequency of the gain spectrum can be tuned by varying the pump power. We provide analytical results and thorough numerical simulations, in excellent agreement, to underscore this observation. As we explain in Section 2, this effect, first reported in this work to the best of our knowledge, is expected to become more apparent in waveguides in the mid-IR spectral range, where the incidence of self-steepening is greatly enhanced due to the smaller optical frequencies and the high nonlinear coefficients typical of materials transparent in this spectral window [18]. In this sense, this tunable Raman gain may find application in mid-IR fiber lasers [19,20], supercontinuum generation, and ultra-wideband slow-light Raman-based devices for all-optical signal processing [21–24].

We point out that the interplay between modulation instability and Raman scattering has previously been addressed in the literature (see, e.g., [25,26] and references therein). In particular, Dinda *et al.* [26] have thoroughly analyzed the interaction between MI and the delayed Raman response in optical fibers, but they did not include the effect of self-steepening in their analysis.

The rest of the paper is organized as follows. In Section 2, we briefly review the numerical model, based on the generalized

nonlinear Schrödinger equation, and revisit analytical expressions for a full model of scalar modulation instability in waveguides. In Section 3, we discuss simulation results in the normal and anomalous dispersion regimes and characterize the tunable gain. Concluding remarks are presented in Section 4.

2. FULL MODEL OF THE SCALAR MODULATION INSTABILITY GAIN

Wave propagation in a lossless nonlinear medium is well described by the generalized nonlinear Schrödinger equation (GNLSE) [27]

$$\frac{\partial A(z,T)}{\partial z} - i\hat{\beta}A(z,T) = i\hat{\gamma}A(z,T)\int_{-\infty}^{\infty} R(T')|A(z,T-T')|^2 \mathrm{d}T', \quad (1)$$

where $A(z,T)$ is the slowly varying envelope, z is the spatial coordinate, and T is the time coordinate in a co-moving frame at the group velocity ($=\beta_1^{-1}$). $\hat{\beta}$ and $\hat{\gamma}$ are operators related to the dispersion and nonlinearity, respectively, and are defined by

$$\hat{\beta} = \sum_{m\geq 2} \frac{i^m}{m!}\beta_m \frac{\partial^m}{\partial T^m}, \qquad \hat{\gamma} = \sum_{n\geq 0} \frac{i^n}{n!}\gamma_n \frac{\partial^n}{\partial T^n}. \quad (2)$$

Here, β_m are the coefficients of the Taylor expansion of the propagation constant $\beta(\omega)$ around a central frequency ω_0. Similarly, γ_n are the coefficients of the Taylor expansion of the nonlinear parameter. It is usually sufficient to consider the expansion up to the first term, that is, $\hat{\gamma} = \gamma_0(1 + i\tau_{\mathrm{sh}}\frac{\partial}{\partial T})$, where τ_{sh} is a timescale related to self-steepening and shock formation [27].

The function $R(T)$ includes the instantaneous (electronic) and delayed Raman response of the medium:

$$R(T) = (1 - f_R)\delta(T) + f_R h_R(T), \quad (3)$$

where f_R weights the two contributions. In the simulations, we use the damped-oscillator approximation for the time-domain delayed response function $h_R(t)$ characterized by the time constants τ_1 and τ_2 and given by [27]

$$h_R(t) = \frac{\tau_1^2 + \tau_2^2}{\tau_1 \tau_2^2} e^{-\frac{t}{\tau_2}} \sin\left(\frac{t}{\tau_1}\right)\Theta(t), \quad (4)$$

where $\Theta(t)$ is the unit step function.

A straightforward way to characterize the Raman response of the transmission waveguide consists in launching a continuous wave (CW) pump along with broad-bandwidth noise. We expect noise to "copy" the gain spectrum after propagation over some characteristic length and as long as the pump is weakly depleted (i.e., a linear amplifier in the small input-signal regime). In our case, the gain provided by the medium depends upon the interplay between MI and Raman, and, as such, the actual dispersion profile of the waveguide plays a pivotal role. In the normal dispersion region gain is provided only through the Raman response, and noise amplification is described by the Raman coefficient $g_R(\Omega)$, proportional to the imaginary part of $\tilde{h}_R(\Omega) = \mathcal{F}\{h_R(t)\}$ [28] (where $\mathcal{F}$ stands for the Fourier transform):

$$g_R(\Omega) \propto \mathrm{Im}\{\tilde{h}_R(\Omega)\} = \frac{2\Omega\omega_2\omega_1^2}{(\omega_1^2 - \Omega^2)^2 + (2\Omega\omega_2)^2}, \quad (5)$$

where $\Omega = \omega - \omega_0$ is the relative frequency, $\omega_1^2 = \frac{\tau_1^2+\tau_2^2}{\tau_1^2\tau_2^2}$ and $\omega_2 = \tau_2^{-1}$.

Now we turn our attention to the anomalous dispersion region, where the waveguide provides both modulation instability and Raman gain. The instability gain is obtained as [14]

$$g(\Omega) = -2\mathrm{Im}\{K_{1,2}(\Omega)\}, \quad (6)$$

where $K_{1,2}(\Omega)$ is given by

$$K_{1,2}(\Omega) = \tilde{\beta}_o + P_0\gamma_0\tau_{\mathrm{sh}}\Omega(1+\tilde{R}) \pm \sqrt{(\tilde{\beta}_e + 2\gamma_0 P_0\tilde{R})\tilde{\beta}_e + P_0^2\gamma_0^2\tau_{\mathrm{sh}}^2\Omega^2\tilde{R}^2}. \quad (7)$$

Here, $\tilde{\beta}_e = \sum_{n\geq 1}\frac{\beta_{2n}}{(2n)!}\Omega^{2n}$ and $\tilde{\beta}_o = \sum_{n\geq 1}\frac{\beta_{2n+1}}{(2n+1)!}\Omega^{2n+1}$ are even and odd dispersion operators, respectively. In the absence of Raman ($f_R = 0$), the self-steepening effect imposes a cutoff power, above which the MI gain is suppressed, given by [16]

$$P_{\mathrm{cutoff}} = \frac{|\beta_2|}{\gamma_0\tau_{\mathrm{sh}}^2}, \quad (8)$$

when higher-order dispersion terms are neglected. In terms of the normalized power $p = \frac{P_0}{P_{\mathrm{cutoff}}}$, this means that there is no significant MI gain for $p > 1$ even when $f_R > 0$. The self-steepening term can be thought of as an additional dispersive term that depends on both P_0 and ω_0. This leads to the "effective" dispersion taking positive values, thus canceling the MI gain.

Because the cutoff power decreases with increasing nonlinearity (γ_0), and τ_{sh} is usually well approximated by ω_0^{-1}, we expect the MI cutoff phenomenon to be more relevant for highly nonlinear waveguides and for longer wavelengths. For this reason, we focus on the mid-IR range and use parameters consistent with those of waveguides made of chalcogenide glasses, which have low absorption coefficients in the mid-IR and Kerr nonlinear coefficients up to a thousand times higher than that of silica (see [18] and references therein).

The effect of the MI cutoff is portrayed in Fig. 1 for a pump in the mid-IR ($\lambda_0 = 5$ μm).

Propagation is simulated using the GNLSE for a generic waveguide of constant effective area, whose physical parameters are consistent with those found in the literature. These are $\gamma_0 = 100\ \mathrm{W}^{-1}\ \mathrm{km}^{-1}$, $\tau_{\mathrm{sh}} = \omega_0^{-1}$, $\beta_2 = -50\ \mathrm{ps}^2/\mathrm{km}$, and, for the sake of simplicity, $\beta_k = 0$ for $k > 2$. The chosen value of γ_0 is consistent with that of a chalcogenide waveguide in the mid-IR around 5 μm [18]. For the Raman response, we use Eqs. (3) and (4) with $f_R = 0.031$, $\tau_1 = 15.5$ fs and $\tau_2 = 230.5$ fs, values in agreement with those found in the literature for chalcogenide glasses [29].

Because there is no significant MI gain for $p > 1$, we expect to recover the same results as in the normal dispersion regime when injecting pump plus noise into the waveguide. Because we only consider the effect of dispersion up to the second order, β_2, we may rewrite Eq. (7) in terms of p as

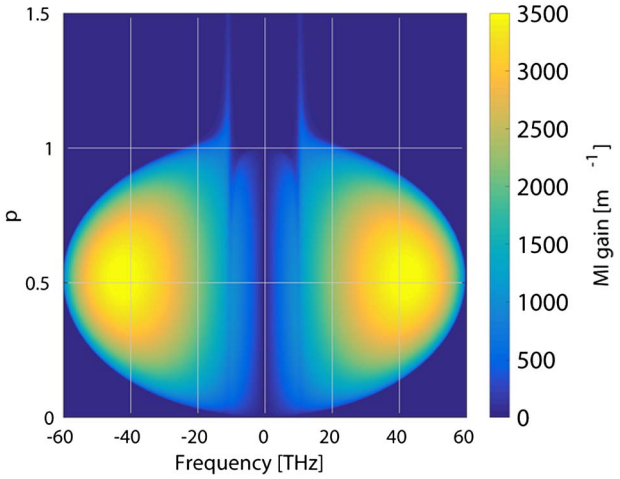

Fig. 1. Modulation instability gain versus p in the frequency range of interest. Frequency at 0 THz corresponds to a pump wavelength of 5 μm.

$$K_{1,2}(\Omega,p)=\frac{p|\beta_2|}{\tau_{sh}}\Omega(1+\tilde{R})\pm|\beta_2\Omega|\sqrt{\frac{\Omega^2}{4}-\frac{p\tilde{R}}{\tau_{sh}^2}+\frac{p^2\tilde{R}^2}{\tau_{sh}^2}}. \tag{9}$$

Hence, the instability gain is given by

$$g(\Omega,p)=-2\mathrm{Im}\{K_{1,2}(\Omega,p)\}. \tag{10}$$

As we are interested in the amplification of the output signal after a traveled distance L into the waveguide, we compute the total power gain $G=e^{2g(\Omega,p)L}$ as a function of the normalized pump power p. Results are displayed in Fig. 2, where different spectra are shown at a constant total power gain. The corresponding Raman gain, i.e., $e^{2g_R(\Omega)L}$, is also shown for comparison. It can be readily observed that we are in the presence of a power-controlled gain that approaches the Raman gain as p increases. This in fact can be thought of as a *pump-tunable Raman gain*.

3. NUMERICAL RESULTS

We solve the propagation equation [Eq. (1)] using the embedded fourth-order Runge–Kutta in the interaction picture method [30]. In Fig. 3 we show simulations results of launching a CW pump along with white Gaussian noise (pump-to-noise ratio is set at 40 dB.) The spectrum shown is the average over 50 noise realizations. The input pump power is $P_0=1000$ W, and the waveguide parameters are the same as those used for Fig. 1, except for the dispersion coefficient $\beta_2=50$ ps^2/km, which is purposely chosen to greatly reduce the efficiency of four-wave mixing interactions. The waveguide length was set to $L=10$ mm. We must note that, although pump powers of the order of the kilowatt may be unrealistic in the CW regime, they can be easily achieved in a quasi-CW regime, i.e., with nano- or picosecond pulses [31,32].

We can readily observe that the noise spectral distribution closely follows that expected from the Raman gain. Indeed, we can fit the normalized noise output and use it to obtain the characteristic parameters of the Raman gain spectrum. From the numerical fit, we obtain $\omega_1/2\pi=-10.36$ THz and $\omega_2/2\pi=0.67$ THz, in excellent agreement with the assumed Raman response ($\omega_1/2\pi=-10.29$ THz and $\omega_2/2\pi=0.69$ THz), validating this scheme as a way to measure the unknown Raman response of an arbitrary waveguide.

Now we turn our attention to the anomalous regime ($\beta_2=-50$ ps^2/km). Results for two different normalized pump powers are shown in Figs. 4 and 5. In both cases, the length of the waveguide is 7 L_{MI}, where $L_{MI}=[\max\{g(\Omega,p)\}]^{-1}$ is the modulation instability length. Interestingly, the noise

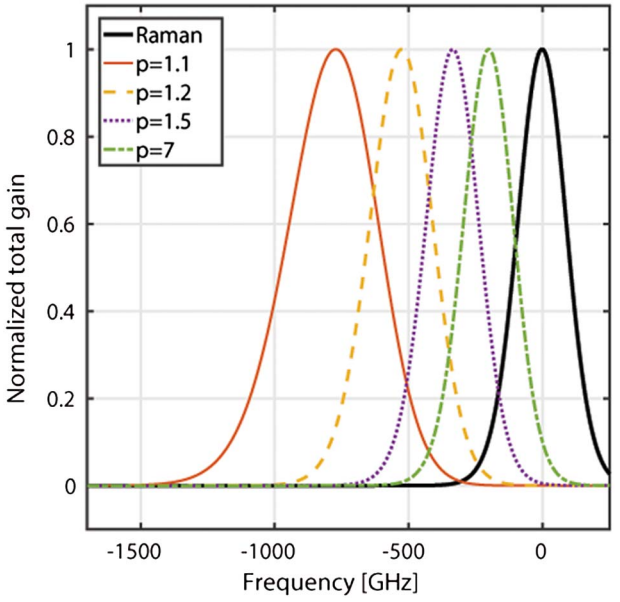

Fig. 2. MI gain for some values of p and for $f<0$ (relative frequency from the Raman-gain peak). Observe that the gain profile is essentially that of Raman but *rendered tunable*.

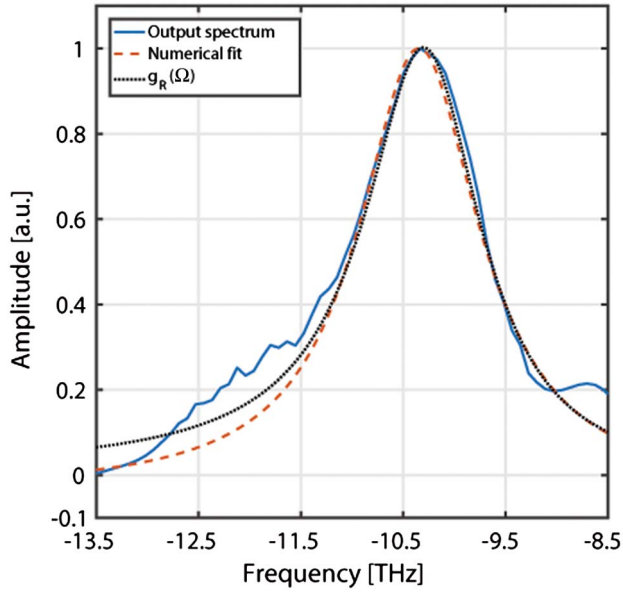

Fig. 3. Output spectrum averaged over 50 noise realizations, numerical fit of the average spectrum, and normalized Raman gain coefficient, g_R.

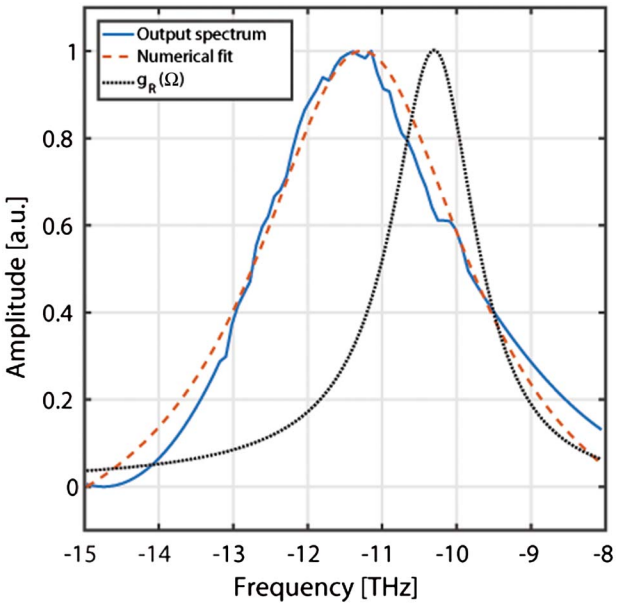

Fig. 4. Average spectrum, numerical fit, and normalized Raman gain for $p = 1.1$.

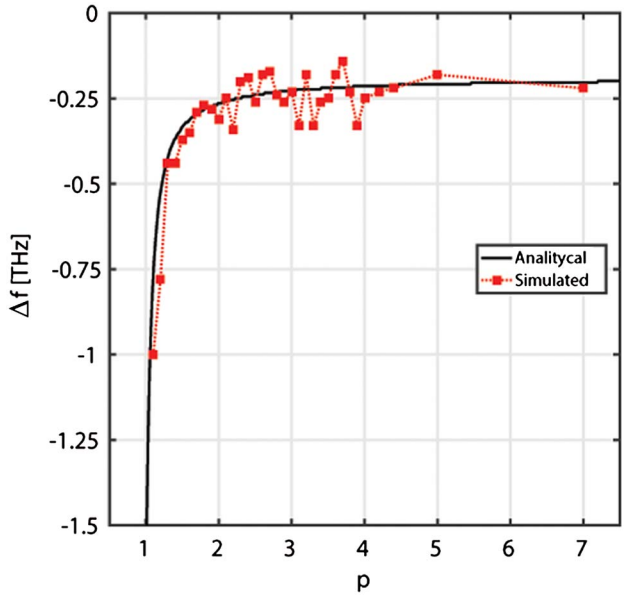

Fig. 6. Raman frequency shift versus normalized power, p.

output spectrum continues to follow the Raman gain profile; therefore, Raman response data can still be inferred from it, but it appears shifted in frequency. The higher the pump power, the closer the peak gain approaches that of the normal dispersion regime.

For pump levels much lower than the MI cutoff power, the gain spectrum is dominated by MI, and launching noise along with the pump cannot be effectively used to determine the Raman response of the waveguide. However, close to and above the cutoff power, the spectral signature is driven by the Raman response, centered at different frequencies. This behavior is further illustrated in Fig. 6, where we show analytical results for the Raman-gain peak shift [obtained from Eq. (10)] and numerical simulations, averaged over many noise realizations, as a function of the normalized pump power p. Note that fluctuations observed in the numerical results are due to the chosen frequency discretization and the limited number of averaged noise realizations. In all cases, the propagated distance is $7\ L_{MI}$.

An interesting example of an application of this tunable gain is shown Fig. 7, where a strong pump is launched into the waveguide together with two seed signals, which are expected

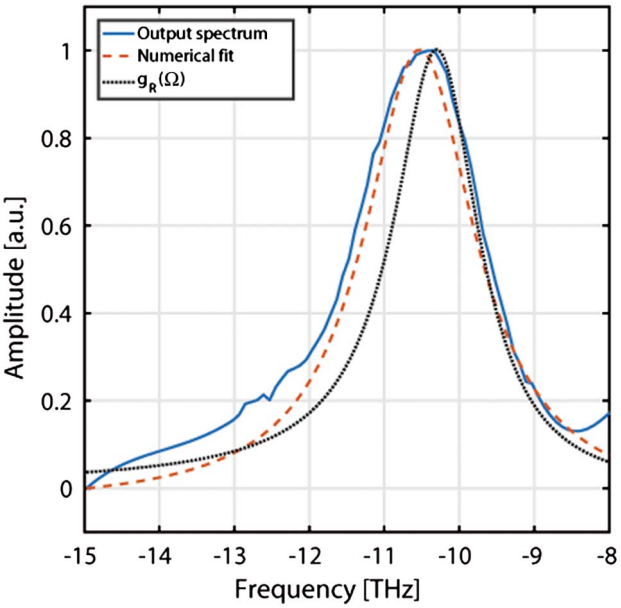

Fig. 5. Average spectrum, numerical fit, and normalized Raman gain for $p = 7$.

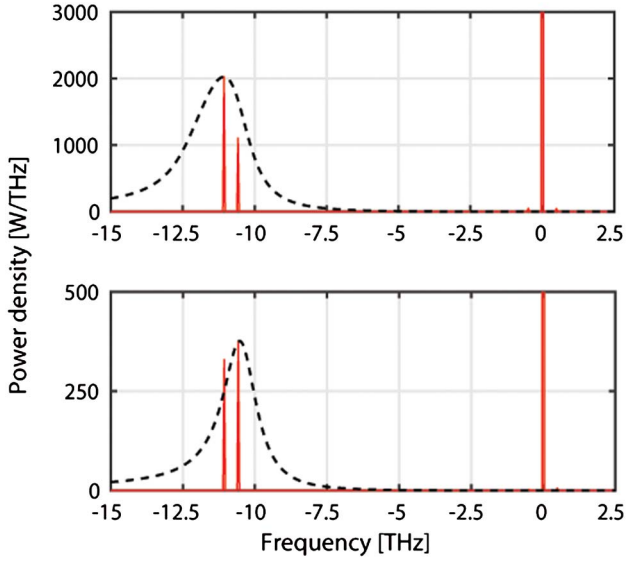

Fig. 7. Output spectra after a propagated distance of 3.6 mm. The input to the waveguide is a pump plus two small seed signals (40 dB below pump level to avoid pump depletion). $p = 1.1$ (top) and $p = 3.0$ (bottom). The pump power is used to select which signal is favored via Raman amplification.

to be amplified by the pump via Raman interaction. The seed signal power was chosen at 40 dB below the pump level in order to remain within the undepleted approximation and also to avoid the appearance of four-wave mixing products at the propagated distance of 3.6 mm. The pump power was chosen such that $p = 1.1$ (top panel) and $p = 3.0$ (bottom panel). We observe that the pump power can be effectively used to select which signal will grow the most by tuning the Raman peak gain to the frequency of interest.

4. CONCLUSIONS

In summary, in this paper we put forth an analysis of the interplay among Raman gain, dispersion, and self-steeping in a full model of modulation instability in waveguides. The effect of self-steepening enables a power cutoff above which the gain is expected to be dominated by the Raman response of the medium. A close examination of the region around this cutoff revealed a striking feature, namely, that there exists a range of pump powers where the Raman spectrum can be tuned at will. Analytical and numerical results, in excellent agreement, were presented to confirm this, as far as we know, original observation. We expect this effect to be of relevance in a wide number of applications, ranging from mid-IR fiber Raman lasers and supercontinuum generation, to ultra-wideband slow-light Raman-based devices for all-optical signal processing.

REFERENCES

1. A. Hasegawa and W. Brinkman, "Tunable coherent IR and FIR sources utilizing modulational instability," IEEE J. Quantum Electron. **16**, 694–697 (1980).
2. D. Anderson and M. Lisak, "Modulational instability of coherent optical-fiber transmission signals," Opt. Lett. **9**, 468–470 (1984).
3. K. Tai, A. Hasegawa, and A. Tomita, "Observation of modulational instability in optical fibers," Phys. Rev. Lett. **56**, 135–138 (1986).
4. M. Nakazawa, K. Suzuki, H. Kubota, and H. A. Haus, "High-order solitons and the modulational instability," Phys. Rev. A **39**, 5768–5776 (1989).
5. A. Demircan and U. Bandelow, "Supercontinuum generation by the modulation instability," Opt. Commun. **244**, 181–185 (2005).
6. J. M. Dudley, G. Genty, F. Dias, B. Kibler, and N. Akhmediev, "Modulation instability, Akhmediev breathers and continuous wave supercontinuum generation," Opt. Express **17**, 21497–21508 (2009).
7. D. Solli, C. Ropers, P. Koonath, and B. Jalali, "Optical rogue waves," Nature **450**, 1054–1057 (2007).
8. K. Hammani, C. Finot, B. Kibler, and G. Millot, "Soliton generation and rogue-wave-like behavior through fourth-order scalar modulation instability," IEEE Photon. J. **1**, 205–212 (2009).
9. N. Akhmediev, J. M. Soto-Crespo, and A. Ankiewicz, "How to excite a rogue wave," Phys. Rev. A **80**, 043818 (2009).
10. S. T. Sørensen, C. Larsen, U. Møller, P. M. Moselund, C. L. Thomsen, and O. Bang, "Influence of pump power and modulation instability gain spectrum on seeded supercontinuum and rogue wave generation," J. Opt. Soc. Am. B **29**, 2875–2885 (2012).
11. V. Zakharov and A. Gelash, "Freak waves as a result of modulation instability," Procedia IUTAM **9**, 165–175 (2013).
12. S. Toenger, T. Godin, C. Billet, F. Dias, M. Erkintalo, G. Genty, and J. M. Dudley, "Emergent rogue wave structures and statistics in spontaneous modulation instability," Sci. Rep. **5**, 10380 (2015).
13. P. Béjot, B. Kibler, E. Hertz, B. Lavorel, and O. Faucher, "General approach to spatiotemporal modulational instability processes," Phys. Rev. A **83**, 013830 (2011).
14. J. Bonetti, S. M. Hernandez, P. I. Fierens, and D. F. Grosz, "Analytical study of coherence in seeded modulation instability," Phys. Rev. A **94**, 033826 (2016).
15. P. K. Shukla and J. J. Rasmussen, "Modulational instability of short pulses in long optical fibers," Opt. Lett. **11**, 171–173 (1986).
16. C. D. Angelis, G. Nalesso, and M. Santagiustina, "Role of nonlinear dispersion in the dynamics of induced modulational instability in kerr media," J. Opt. Soc. Am. B **13**, 848–855 (1996).
17. F. Koch, S. A. E. Lewis, S. V. Chernikov, and J. R. Taylor, "Broadband raman gain characterisation in various optical fibres," Electron. Lett. **37**, 1437–1439 (2001).
18. B. J. Eggleton, B. Luther-Davies, and K. Richardson, "Chalcogenide photonics," Nat. Photonics **5**, 141–148 (2011).
19. S. D. Jackson, "Towards high-power mid-infrared emission from a fibre laser," Nat. Photonics **6**, 423–431 (2012).
20. M. Bernier, V. Fortin, N. Caron, M. El-Amraoui, Y. Messaddeq, and R. Vallée, "Mid-infrared chalcogenide glass Raman fiber laser," Opt. Lett. **38**, 127–129 (2013).
21. J. E. Sharping, Y. Okawachi, and A. L. Gaeta, "Wide bandwidth slow light using a Raman fiber amplifier," Opt. Express **13**, 6092–6098 (2005).
22. Y. Okawachi, M. A. Foster, J. E. Sharping, A. L. Gaeta, Q. Xu, and M. Lipson, "All-optical slow-light on a photonic chip," Opt. Express **14**, 2317–2322 (2006).
23. K. Suzuki and T. Baba, "Nonlinear light propagation in chalcogenide photonic crystal slow light waveguides," Opt. Express **18**, 26675–26685 (2010).
24. O. D. Herrera, L. Schneebeli, K. Kieu, R. A. Norwood, and N. Peyghambarian, "Slow light based on stimulated Raman scattering in an integrated liquid-core optical fiber filled with cs2," Opt. Express **21**, 8821–8830 (2013).
25. E. A. Golovchenko and A. N. Pilipetskii, "Unified analysis of four-photon mixing, modulational instability, and stimulated Raman scattering under various polarization conditions in fibers," J. Opt. Soc. Am. B **11**, 92–101 (1994).
26. P. T. Dinda, C. Ngabireng, K. Porsezian, and B. Kalithasan, "Modulational instability in optical fibers with arbitrary higher-order dispersion and delayed Raman response," Opt. Commun. **266**, 142–150 (2006).
27. G. Agrawal, *Nonlinear Fiber Optics*, 5th ed., Optics and Photonics (Academic, 2012).
28. R. H. Stolen, W. J. Tomlinson, H. A. Haus, and J. P. Gordon, "Raman response function of silica-core fibers," J. Opt. Soc. Am. B **6**, 1159–1166 (1989).
29. M. R. Karim, B. M. A. Rahman, and G. P. Agrawal, "Mid-infrared supercontinuum generation using dispersion-engineered $Ge_{11.5}As_{24}Se_{64.5}$ chalcogenide channel waveguide," Opt. Express **23**, 6903–6914 (2015).
30. J. Hult, "A fourth-order Runge-Kutta in the interaction picture method for simulating supercontinuum generation in optical fibers," J. Lightwave Technol. **25**, 3770–3775 (2007).
31. X. Gai, D.-Y. Choi, S. Madden, Z. Yang, R. Wang, and B. Luther-Davies, "Supercontinuum generation in the mid-infrared from a dispersion-engineered As_2S_3 glass rib waveguide," Opt. Lett. **37**, 3870–3872 (2012).
32. Y. Yu, X. Gai, T. Wang, P. Ma, R. Wang, Z. Yang, D.-Y. Choi, S. Madden, and B. Luther-Davies, "Mid-infrared supercontinuum generation in chalcogenides," Opt. Mater. Express **3**, 1075–1086 (2013).